APPLIED PHYSICS

Frictional weakening of slip interfaces

B. Weber[1,2]*, T. Suhina[1,3], A. M. Brouwer[3], D. Bonn[1]*

When two objects are in contact, the force necessary to overcome friction is larger than the force necessary to keep sliding motion going. This difference between static and dynamic friction is usually attributed to the growth of the area of real contact between rough surfaces in time when the system is at rest. We directly measure the area of real contact and show that it actually increases during macroscopic slip, despite the fact that dynamic friction is smaller than static friction. This signals a decrease in the interfacial shear strength, the friction per unit contact area, which is due to a mechanical weakening of the asperities. This provides a novel explanation for stick-slip phenomena in, e.g., earthquakes.

INTRODUCTION

Earthquakes are known to result from the stick-slip motion of Earth's crust, a mechanical instability that is driven by the reduction of friction at the onset of sliding motion (*1*–*3*). This difference between static and dynamic friction can be observed in virtually all frictional systems and is captured by the "state" term in rate and state friction theory: The static friction force increases as the logarithm of the time both surfaces have spent in contact (*4*–*10*). While rate and state friction theory successfully describes the history and velocity dependence of the friction force in many systems, the microscopic mechanisms that drive this empirical model remain elusive. Adhesive friction originates at—and is presumed to be proportional to—the area of real contact, the molecular area over which surface roughness peaks touch. This area of real contact is often described as a collection of discrete contact points, also known as single-asperity contacts (*11*–*16*). At a multiasperity interface, the contact force deforms the surface roughness, leading to elastic deformations at various length scales and local stresses that can approach the yield stress of the materials involved (*17*–*19*). Under the influence of these high stresses, contacting materials undergo creep deformation, resulting in growth of the area of real contact with time (*4*, *20*, *21*). This geometrical aging is thought to strongly contribute to the logarithmic growth of the static friction force with rest time observed in many friction experiments (*4*–*10*). However, direct observation of the area of real contact at multiasperity interfaces is experimentally challenging (*4*, *10*, *22*–*25*) because the frictional interface is buried between two bulk phases and the length scales involved are small.

Here, we show that the transition from static to dynamic friction is not caused by a reduction in the number of touching asperities but by slip weakening of those same asperities. At rest, the asperities harden again: This is the aging that leads to a higher static friction coefficient. We measure the true contact area for a multiasperity system using surface-immobilized molecules that fluoresce brightly when spatially confined in a contact. For our polystyrene (PS)–on-glass contacts, slide-hold-slide friction experiments show that, contrary to what is commonly assumed, the contact area actually increases as the friction force decreases from its static to its dynamic value. Because the dynamic friction is smaller than the static friction while the real contact area increases at the point of slippage, the interfacial shear stress, i.e., the friction per unit contact area (σ), has to decrease at this point. The fluorescence intensity of the probe molecules is stronger when the local free volume is smaller, enabling us to show that the PS interface is compact at rest (higher σ) and dilates (lower σ) during slip, causing the slip weakening. The difference between static and dynamic friction is therefore not controlled by the size of the area of real contact but by its interfacial shear stress. Since glassy interfaces are ubiquitous (e.g., in earthquakes), this has far-reaching consequences for our understanding of frictional slip.

RESULTS

In the friction experiments, we bring a 600-μm-diameter rough PS sphere into contact with a very flat and smooth float glass coverslip coated with a monolayer of pressure-sensitive molecules (Fig. 1). Contact mechanics models usually map the situation of two rough surfaces in contact onto that of only a single rough surface on a smooth one, which corresponds to the rough-on-smooth situation we investigate here. The sphere is glued off-center to the bottom of a rheometer plate and is lowered into contact with the coverslip (Fig. 1B). Through rotation of the tool, the rheometer can move the sphere tangentially, while simultaneously measuring both normal (load) and tangential (frictional) forces on the contact. In a single friction test, we rotate the rheometer tool such that a speed of 1 μm/s is imposed on the sphere for a total time of 13 s. Initially, however, this deformation is elastically accommodated by the measurement system, and the sphere does not actually slide (linear buildup in Fig. 1A). Once the static friction force is exceeded, macroscopic slip occurs (peak force in Fig. 1A). Static friction now evolves into dynamic friction, and the plateau value of the friction force is the force required to keep the frictional motion going at a constant sliding speed. We repeat the friction measurements consecutively for the same contact and continue to apply a constant normal force of 400 mN between friction measurements. The observation is that not only the static friction but also the dynamic friction increases roughly as the logarithm of the time that has elapsed since the contact was formed (Fig. 1).

As already mentioned, the increase in static friction in time (*4*–*9*) is commonly believed to be due to the growth of the area of real contact, attributed to creep deformation of asperities in contact. To probe the contact area, a monolayer of stress-sensitive fluorescent molecules is covalently bonded to the glass substrate (*26*, *27*), and the PS sphere-on-glass contact is illuminated from below by confocal laser scanning microscopy (Fig. 1B). Only molecules that are confined by real contact between sphere and glass emit an increased fluorescence intensity (*18*, *26*) that is captured by the inverted microscope (Fig. 1). The fluorescence image of the contact taken with the microscope therefore

[1]Van der Waals–Zeeman Institute, Institute of Physics, University of Amsterdam, Science Park 904, 1098 XH Amsterdam, Netherlands. [2]Advanced Research Center for Nanolithography (ARCNL), Science Park 110, 1098 XG Amsterdam, Netherlands. [3]Van't Hoff Institute for Molecular Sciences, University of Amsterdam, Science Park 904, 1098 XH Amsterdam, Netherlands.
*Corresponding author. Email: bweber.bart@gmail.com (B.W); d.bonn@uva.nl (D.B.)

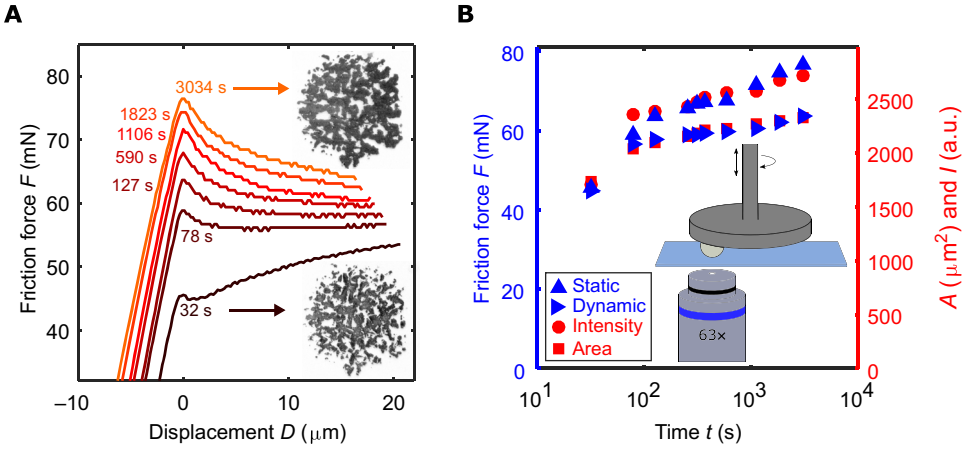

Fig. 1. Time evolution of the friction force and the area of real contact. (**A**) Original friction curves and inverted fluorescence images (75 μm by 75 μm) of the real contact area taken before the first and the last friction test. Fluorescence images of the contact were recorded seconds before the friction measurement was started. (**B**) Real contact area *A* (red squares) measured before the onset of sliding, arbitrarily scaled total fluorescence intensity *I* (red circles) and static (blue triangles pointing up) or dynamic (blue triangles pointing right) friction force *F* as a function of the time elapsed since the contact was initially formed [same data as (A)]. The background fluorescence is measured and subtracted from the intensity values reported in (B). The friction/microscopy setup is schematically shown in the inset in (B). The distance between the sphere center and the rotation axis of the rheometer is more than two orders of magnitude larger than the size of the contact or the sliding distance for a single friction test. Contacts were immersed in formamide to avoid strong light scattering at the interface. Dry experiments, or experiments on glass without rigidochromic molecules, reveal identical frictional behavior (fig. S5). a.u., arbitrary units.

reveals the area of real contact measured with molecular (nanometer) resolution along the normal (*z* direction) and diffraction-limited resolution in the in-plane directions. Considerable surface roughness—and therefore contact area structure—can, in principle, exist at lateral scales that are not resolved by the microscope (*28*). To investigate the presence of such unresolved contact area structure, we complement the contact area observations with contact calculations. As input, the contact calculations use atomic force microscopy (AFM) topographs recorded on the PS sphere surface at the exact location that touches the smooth glass substrate in the visualization experiments. We find that the contact calculation only matches the experimental observation of the area of real contact when both elastic and plastic deformation of the surface roughness are included (Fig. 2). The difference between AFM topographs recorded before and after the contact experiment confirms that there is substantial plastic deformation of the PS surface (Fig. 2B). We previously showed (*18*) that the nature of this plasticity is strain hardening; as the plastic deformation of the PS surface builds up, it hardens. We mimic the limited resolution of the microscope by convoluting the calculated contact areas with Gaussian point spread functions (PSFs) of varying width (Fig. 2C). The important observation is that because of the plastic flattening of the asperities, the contact area does not contain small-scale structure and is therefore fully resolved by the microscope, making the PS-on-glass system ideal for disentangling the relative contributions of geometric and structural aging to the evolution of the friction force.

We track the growth of the area of real contact with time using the fluorescence images. As the sphere is pressed onto the substrate with a constant normal force of 400 mN for a total time of 50 min, we observe a linear increase in contact area with the logarithm of time (Fig. 3A). We now repeat this experiment but additionally impose frictional slip right after the recording of each of the fluorescence images in the time series. Like before, in each of these slip events, a sliding speed of 1 μm/s is imposed on the sphere for 13 s. We continue to measure the age of the contact relative to the moment the contact was formed, rather than relative to the moment when sliding stopped in the previous slip event. The sliding results in an accelerated growth of the area of real contact, particularly for the first slip event that the contact undergoes (just after 32 s). However, the logarithmic growth rate observed in the static experiment also applies to the slide-hold-slide experiment after the first two slip events (Fig. 3A). To visualize the spatial distribution of the contact area growth, we align and subtract the contact areas measured at the beginning (36 s) and end (2992 s) of the static aging experiment (black circles in Fig. 3A). As the normal stress is maximal at the center of a sphere-on-flat contact, substantial growth of the contact area through creep flattening of the roughness can be expected in this region. Unexpectedly, we observe the opposite: Most of the contact area growth occurs at the perimeter of the contact area through flattening of existing contacts (Fig. 3B). We now apply the exact same analysis to the contact areas that were measured before (32 s) and after (78 s) the first slip event in the slide-hold-slide experiment. The growth in contact area in this 46-s time window is roughly equal to the growth observed over 50 min during the static aging experiment. The spatial distribution of this accelerated contact area growth is identical to the one found in the static aging experiment, suggesting that the mechanism that drives the growth in contact area is the same in both cases (Fig. 3B). Furthermore, the direction in which the friction force was applied does not seem to influence the contact area growth; apparently, this growth is not a consequence of shear forces acting on the interface. Instead, we argue that the growth of the area of contact under the influence of externally applied normal and tangential forces is a consequence of the creep deformation of the bulk sphere material: The external forces cause the sphere to flatten in time, thereby creating contacts at the perimeter of the contact area. The central question is then whether the time dependence of static friction (*4*–*9*) is caused by this growth of the area of real contact. In Fig. 1B, we plot the static friction force together with the area of real contact measured right before each friction test performed in the slide-hold-slide series. The important observation is that the static friction increases faster than the area of real contact: This means that the friction per unit contact area increases. It increases here from $\sigma = 28$ MPa after 30 s to $\sigma = 33$ MPa after more than an hour of aging. Both values are within 10% of the shear strength of

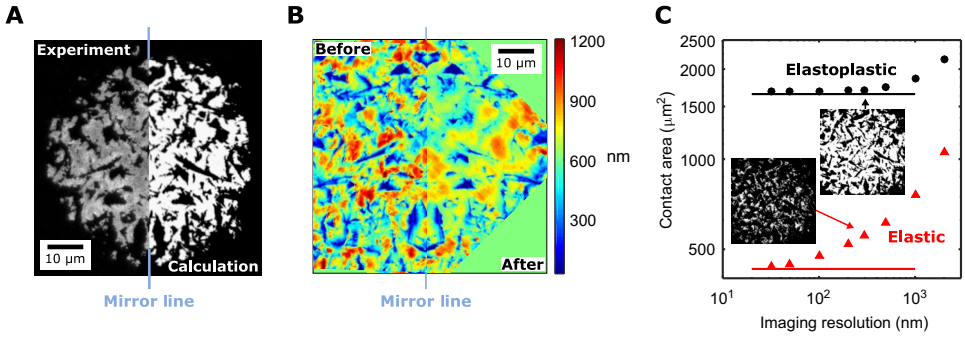

Fig. 2. The area of real contact. (**A**) Half of the fluorescence image (left) and the mirrored elastoplastic contact calculation (right) of the rough PS on smooth glass contact at a normal force of 392 mN. The plasticity is modeled by increasing the gap at which contact is defined in the purely elastic calculation from 0.1 to 170 nm: This is the only adjustable parameter, and the plain strain modulus is independently measured (*18*): E^* = 3.7 GPa. (**B**) The AFM topograph of the PS sphere before (left) and after (right; mirrored, areas outside AFM range shown in green) contact with glass shows plastic deformation of the same order. Before the contact experiment, the root mean square roughness of the sphere is 650 nm, and that of the substrate is 2 nm (fig. S4). (**C**) Calculated contact area as a function of the full width half maximum of the Gaussian PSF with which the contact area is convolved. The AFM and contact calculations both have a pixel size of 32 nm, roughly an order of magnitude lower than the microscopy PSF. The sphere curvature was subtracted from the AFM topographs shown in (B) to highlight the surface roughness. To define the experimental or calculated and convolved area of real contact, we set an intensity threshold (*38*) and simply multiply the pixel area with the total number of pixels with intensities above the threshold (fig. S1); for all experiments and calculations, the pixel size is smaller than the PSF.

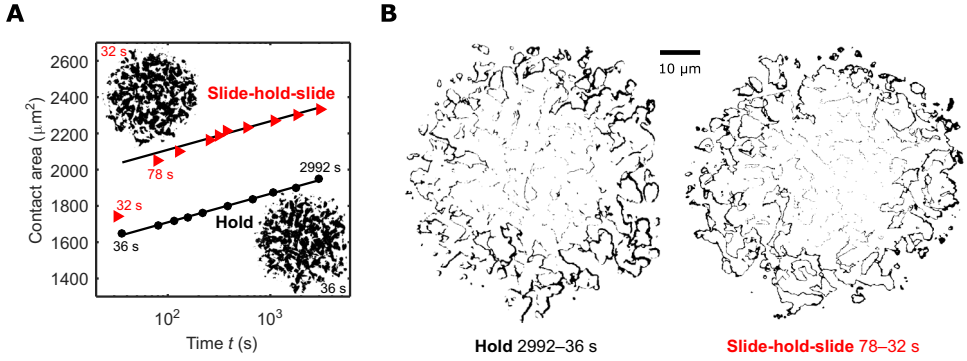

Fig. 3. Contact area growth in time. (**A**) Contact area as a function of the time the sphere has spent in contact with the glass at $N \approx 400$ mN (black circles). The contact area growth is accelerated when slip is imposed right after each contact area measurement (red triangles, time measured relative to the moment of contact formation, not to the end of each slip event) but saturates at the same logarithmic growth rate after the first few slip events (black solid lines). Inset images show contact areas (black areas) corresponding to the first data points. (**B**) Difference images highlighting contact area growth (left) after 50 min of contact (without macroscopic slip) and (right) after the first slip event.

PS (≈30 MPa) so that plastic yielding of the PS seems to be the pertinent physical process. In agreement with this hypothesis, we find that the friction behavior is unchanged when we remove the probe molecules: The friction is controlled by the PS, and the friction mechanism is plastic yielding of a thin PS surface layer (fig. S5) (*21*, *29*, *30*).

The physical process that drives the time evolution of σ is directly revealed by the probe molecules at the interface. The fluorescence intensity of each pixel within the area of real contact is a local measure of the free volume experienced by the probe molecules (fig. S3). Plotting the total fluorescence intensity emitted by the probe molecules right before each friction test in Fig. 1B, we find that the total fluorescence intensity increases in the same manner as the static friction force; in the area of real contact, the fluorescence becomes brighter. This signals a decrease in the free volume experienced by the interfacial probe molecules; the glassy PS surface becomes more compact during aging. This compaction directly affects σ; a more compact interface is mechanically stronger and therefore supports a larger static friction force. A detailed study of the contact mechanics, where the static contact area is measured as a function of the normal force and compared with simulations, also shows that, to quantitatively explain the contact mechanics, strain hardening of the asperities needs to be taken into account (*18*).

The behavior of the friction force is generic for slip events: It increases up to the static limit at which the contact breaks and the sphere starts to slide over the substrate with a smaller friction force (Fig. 4). The transition from static to dynamic friction does not happen over a molecular length scale but gradually occurs as the sphere slides over a distance of several micrometers. To elucidate the physics behind this transition, we consider the area of real contact during interfacial slip. At a rate of 3 frames/s, we record fluorescence images of the contact during a typical slow friction measurement. From these images, we extract the area of real contact, the total fluorescence intensity, and the position of the contact. These quantities are then plotted alongside the simultaneously measured friction force (Fig. 4). As the tangential force builds up toward its peak value, we observe a sudden decrease in contact area, followed by the onset of macroscopic sliding and the

gradual decrease in the friction force from its static to its dynamic value. We first consider the reduction in contact area that is observed before macroscopic slip can be detected. To visualize this change in contact area, we align and subtract the binarized contact images recorded just before and just after the contact area decreases (panel 2-1 in Fig. 5). The difference image reveals two distinct changes: (i) At the perimeter of the overall contact area, trailing edge contacts disappear (red edges on the left in panel 2-1 of Fig. 5) while leading edge contacts grow (blue edges on the right in panel 2-1 of Fig. 5). (ii) Contact patches that are not positioned along the perimeter of the overall contact area all shrink under the influence of the tangential force. Both (i) and (ii) are reversed when the externally applied tangential force is removed: Panel 4-3 in Fig. 5 shows that trailing edge contacts return while leading edge contacts are broken and all other contacts grow (blue edges). Because the changes in contact area at the leading and trailing edge roughly cancel each other out, the drop (rise) in contact area observed before (after) macroscopic slip is a consequence of the shrinking of individual contact patches under the influence of the tangential force. Shear-induced shrinking of the area of contact was, so far, only observed for softer materials in which the effect is much stronger and found to result from a combination of the contacts peeling off at their perimeter (mode I fracture) and contact compression in the tangential loading direction through microslip (*25*, *31*).

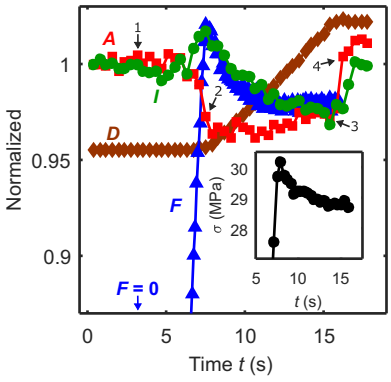

Fig. 4. The stick-slip transition. Normalized contact area (*A*), total fluorescence intensity (*I*), contact displacement (*D*), and friction force (*F*) measured during the 78-s slip event also shown in Fig. 1. The arrows and numbers indicate which data points were used for the difference images in Fig. 5. Contact displacement is measured by optimally overlapping subsequent fluorescence images to the first fluorescence image in the series. Inset shows shear stress σ—defined as the ratio of friction force to real contact area—corresponding to the data in the main figure.

The shear-induced reduction in contact area is accompanied by an overall increase in the fluorescence intensity (Fig. 4). As the tangential force builds up, we first observe this increased fluorescence intensity at the perimeter of the contact area from which it propagates toward the center of the contact. To quantify this, we construct radially averaged intensity profiles for the contact images that were recorded before the onset of macroscopic slip and subtract subsequent profiles (Fig. 6). Earlier experiments (*32*) and simulations (*33*) have demonstrated the nucleation and propagation of slow rupture fronts along frictional interfaces right before the onset of macroscopic motion. These are driven by slow slip, separate microslipping regions of the interface from sticking regions, and can move at velocities orders of magnitude smaller than the material's shear wave speed. We interpret the presented intensity waves in this context since microslip can be expected to initiate at the perimeter of the sphere-on-flat contact, where the shear stresses are maximal and the normal stresses are minimal. The increased fluorescence intensity measured at those contact patches that have been subject to microslip indicates that

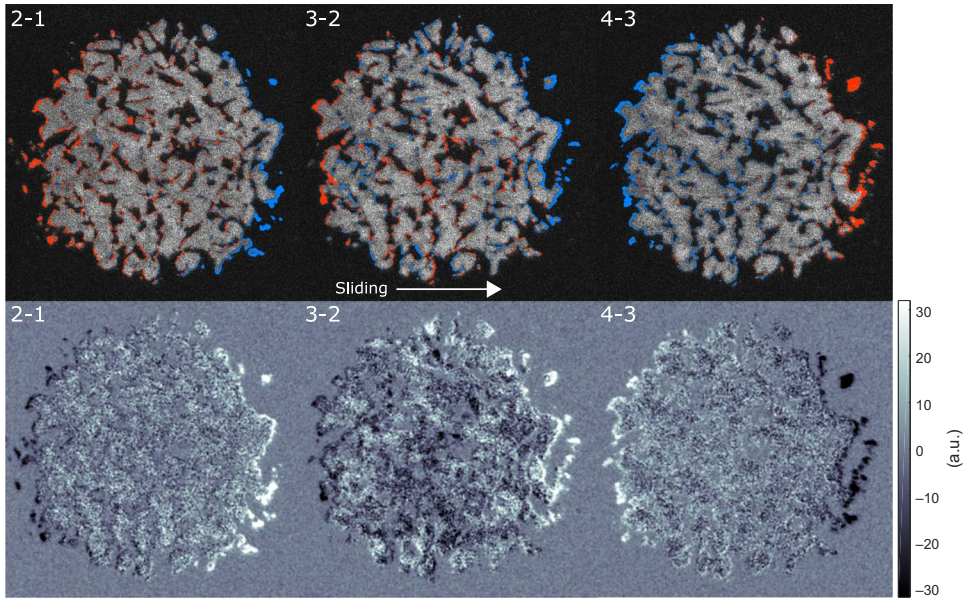

Fig. 5. Difference images corresponding to Fig. 4. Top: Newly formed contacts are shown in blue, and broken contacts are shown in red. **Bottom:** Fluorescence intensity changes. Before sliding starts (2-1), existing contacts shrink under the influence of the tangential force (contact edges turn red), while a slight rolling motion of the sphere causes trailing edge contacts (left) to break and leading edge contacts (right) to form. During macroscopic slip (3-2), leading edge contacts continue to grow, while trailing edge contacts disappear. As sliding stops and the tangential force is removed from the contact (4-3), contacts grow again at the asperity level (contact edges turn blue), while the sphere rotates back to restore the trailing edge contacts that were broken and to remove the leading edge contacts that were formed.

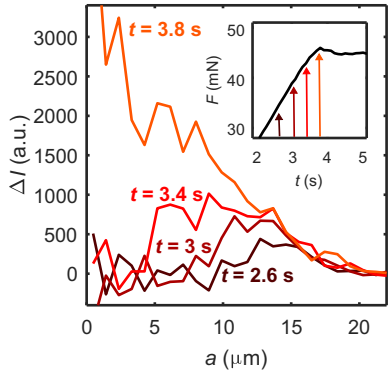

Fig. 6. Contact breaking. The change in fluorescence intensity (Δ*I*) observed at various distances from the contact center (*a*) during the buildup of the static friction force. Inset shows friction force as a function of time, with arrows indicating the moments at which the intensity distributions were recorded. The fluorescence intensity is radially averaged around the center of the contact. As the friction force approaches its static value, a front of increased fluorescence intensity moves from the perimeter of the contact area toward the center at a speed of approximately 10 μm/s.

the pressure-sensitive molecules at the interface experience a higher degree of confinement.

Subsequent to the shear-induced shrinkage of the contact area and the propagation of a rupture front through the entire contact area, macroscopic sliding starts (Fig. 4). We find that although dynamic friction is lower than static friction, the area of real contact actually increases by about 1% during macroscopic slip (Fig. 4). The difference between the two must therefore be controlled by a decrease in σ, the friction force per unit contact area. Using pressure-sensitive molecules at the interface, we demonstrate that the decrease in σ is caused by an increase in free volume at the area of real contact upon sliding; the evolution of the fluorescence intensity perfectly tracks that of the independently measured friction force.

To observe at what locations within the contact area the fluorescence intensity changes, we also construct difference images that highlight the evolution of the fluorescence intensity throughout the friction measurement. The intensity difference image corresponding to the sliding phase (3-2 panel, bottom, in Fig. 5] shows that intensity is lost not only where contacts are destroyed but also mainly at contacts that remain during slip. This drop in fluorescence intensity corresponds to an increase in free volume for the polymers at the interface (*14*). The difference between static and dynamic friction therefore is the result of sliding-induced dilation corresponding to a weakening of the PS surface, an effect that reverses the compaction observed when aging and thereby lowers σ, the interfacial shear stress. The comparison of the area of real contact to the dynamic friction force confirms that when the sliding reaches a steady state, σ is constant (Fig. 1B).

DISCUSSION

In conclusion, the time dependence of friction is controlled by both the size and the mechanical strength of the area of real contact. In our rough-on-smooth system, this contact area is initially formed by elastoplastic deformation of the sphere roughness (*18*) and can subsequently change because of creep deformation of the bulk material. The friction per unit contact area is set by the density of the interfacial PS and increases at rest. This process is reversed when a sufficient tangential force is applied and the contact slips. The observation that the static friction force is larger than the dynamic one is quite general, the detailed mechanism that causes the difference may not be universal; AFM experiments have shown that the formation of chemical bonds across a frictional silica-silica interface can cause a logarithmic increase in static friction with stop time (*8*, *34*); generally, chemical or physical adhesion may be time dependent and change the static and dynamic friction force (*35*). We have shown here that σ, the friction per unit contact area, increases at rest and decreases during slip because of the compaction and dilation, respectively, of amorphous material at the frictional interface. This behavior can be expected at any interface involving contact pressures that approach the material yield stress. Earthquakes, in particular, satisfy this condition as evidenced by the molten rock found along fault lines (*36*, *37*).

MATERIALS AND METHODS

The setup consists of a ZEISS Axiovert 200M LSM 5 Pascal inverted laser scanning confocal microscope on top of which an Anton Paar DSR 301 rheometer is mounted using a custom-made frame. Microbeads TS-500 general-purpose PS spheres of 600 μm in diameter are first roughened by shaking in a container with sandpaper walls (*18*) and then glued to the rheometer tool using epoxy glue. The distance between the rotation axis of the rheometer and the center of the sphere is measured by microscopy. Using this distance, torque and rotation angle values directly measured by the rheometer can be converted to friction forces and distances, respectively.

We covalently attached rigidochromic probe molecules to glass coverslips. The latter were functionalized with *N*-(2-aminoethyl)-3-aminopropyl-trimethoxysilane, and the probes were attached using an amide bond (*18*, *26*).

To image the real contact area (*18*), we first aligned the focal plane of the microscope with the frictional interface. Fluorescence images were then point-scanned using 488-nm excitation light. Contacts were immersed in formamide to avoid strong light scattering at the interface and improve image quality. The area of real contact were measured by applying an Otsu (*38*) threshold to the fluorescence images and multiplying the number of high-intensity pixels with the pixel area (fig. S1). To calculate the total fluorescence intensity *I*, we first measured the average background fluorescence, defined as the average intensity of pixels in the fluorescence image that are not part of the area of real contact. We then multiplied this average background pixel intensity with the number of pixels in the image and subtracted this from the total image intensity to obtain *I*.

In fig. S2, we display the simultaneously measured fluorescence and reflection image of a PS-on-glass contact. At those locations where the gap between the sphere surface and the glass surface is smaller than approximately 80 nm, reflections are suppressed; this is the gap at which the first Newton ring around the contact can be observed (*18*). The reflection image displays a contact area that is similar but somewhat larger than that observed using the fluorescent molecules, as can be expected. More details on the comparison of the fluorescence and reflection observations can be found in (*18*).

In fig. S3, we plotted intensity *I* as a function of the average normal pressure *P*, defined as the ratio of contact force and area of real contact. In the sphere-on-flat contacts considered here, the area of real contact is a sublinear function of the contact force (*18*). *P* can therefore be adjusted simply by changing the contact force. We found that *I* increases as the

square root of P (fig. S3), indicating that a larger contact pressure results in stronger confinement of the rigidochromic molecules at the interface. This is confirmed by comparison of the contact data with fluorescence intensities measured while the rigidochromic molecules are immersed in an organic solvent under varying hydrostatic pressure; in solution, the molecules give an identical response. We therefore concluded that the fluorescence intensity reflects the local free volume, which is reduced when the pressure is increased (*39*). As evidenced by Fig. 4, the local free volume is affected not only by normal stresses but also by tangential stresses.

Through AFM, we imaged the surface topography of the glass coverslips that were used as substrates as well as the PS spheres. The coverslips with and without a monolayer of probe molecules covalently attached are very smooth compared to the PS spheres (fig. S4).

We performed friction measurements following the protocol reported above on glass surfaces with and without a monolayer coating of probe molecules and found identical frictional behavior (fig. S5). Furthermore, we experimentally validated that the presence of a low-viscosity immersion fluid does not affect the frictional behavior (fig. S5C).

The frictional shear stress $\sigma = \frac{F}{A}$ corresponding to the measurements shown in Fig. 1 is plotted in fig. S6. We observed that the dynamic shear stress is constant while the static shear stress increases as the contact ages.

In fig. S7, we plotted the normal force measured during the slip event shown in Fig. 4. We found that the normal force remains constant during the transition from static to dynamic friction. The contact calculations included here were performed using the Tribology Simulator that is publicly available at www.tribonet.org.

SUPPLEMENTARY MATERIALS

Supplementary material for this article is available at http://advances.sciencemag.org/cgi/content/full/5/4/eaav7603/DC1

Fig. S1. Extracting the real contact area from the fluorescence images.
Fig. S2. Fluorescence and reflections observed at a PS-on-glass interface.
Fig. S3. Fluorescence intensity and (normal) pressure.
Fig. S4. Atomic force microscopy.
Fig. S5. Frictional aging on different substrates.
Fig. S6. Frictional shear strength.
Fig. S7. Normal and friction force during slip.

REFERENCES AND NOTES

1. C. H. Scholz, Earthquakes and friction laws. *Nature* **391**, 37–42 (1998).
2. A. Ruina, Slip instability and state variable friction laws. *J. Geophys. Res.* **88**, 10359–10370 (1983).
3. O. M. Braun, I. Barel, M. Urbakh, Dynamics of transition from static to kinetic friction. *Phys. Rev. Lett.* **103**, 194301 (2009).
4. J. H. Dieterich, B. D. Kilgore, Direct observation of frictional contacts: New insights for state-dependent properties. *Pure Appl. Geophys.* **143**, 283–302 (1994).
5. F. Heslot, T. Baumberger, B. Perrin, B. Caroli, C. Caroli, Creep, stick-slip, and dry-friction dynamics: Experiments and a heuristic model. *Phys. Rev. E* **49**, 4973–4988 (1994).
6. J. H. Dieterich, Time-dependent friction in rocks. *J. Geophys. Res.* **77**, 3690–3697 (1972).
7. E. Rabinowicz, The intrinsic variables affecting the stick-slip process. *Proc. Phys. Soc.* **71**, 668 (1958).
8. Q. Li, T. E. Tullis, D. Goldsby, R. W. Carpick, Frictional ageing from interfacial bonding and the origins of rate and state friction. *Nature* **480**, 233–236 (2011).
9. S. Li, Q. Li, R. W. Carpick, P. Gumbsch, X. Z. Liu, X. Ding, J. Sun, J. Li, The evolving quality of frictional contact with graphene. *Nature* **539**, 541–545 (2016).
10. S. Dilavou, S. M. Rubinstein, Nonmonotonic aging and memory in a frictional interface. *Phys. Rev. Lett.* **120**, 224101 (2018).
11. A. M. Homola, J. N. Israelachvili, P. M. McGuiggan, M. L. Gee, Fundamental experimental studies in tribology: The transition from "interfacial" friction of undamaged molecularly smooth surfaces to "normal" friction with wear. *Wear* **136**, 65–83 (1990).
12. G. Reiter, A. L. Demirel, S. Granick, From static to kinetic friction in confined liquid films. *Science* **263**, 1741–1744 (1994).
13. G. Luengo, J. Israelachvili, S. Granick, Generalized effects in confined fluids: New friction map for boundary lubrication. *Wear* **200**, 328–335 (1996).
14. A. Dhinojwala, S. C. Bae, S. Granick, Shear-induced dilation of confined liquid films. *Tribol. Lett.* **9**, 55–62 (2000).
15. P. A. Thompson, G. S. Grest, M. O. Robbins, Phase transitions and universal dynamics in confined films. *Phys. Rev. Lett.* **68**, 3448–3451 (1992).
16. G. He, M. H. Müser, M. O. Robbins, Adsorbed layers and the origin of static friction. *Science* **284**, 1650–1652 (1999).
17. M. H. Müser, W. B. Dapp, R. Bugnicourt, P. Sainsot, N. Lesaffre, T. A. Lubrecht, B. N. J. Persson, K. Harris, A. Bennett, K. Schulze, S. Rohde, P. Ifju, W. G. Sawyer, T. Angelini, H. A. Esfahani, M. Kadkhodaei, S. Akbarzadeh, J.-J. Wu, G. Vorlaufer, A. Vernes, S. Solhjoo, A. I. Vakis, R. L. Jackson, Y. Xu, J. Streator, A. Rostami, D. Dini, S. Medina, G. Carbone, F. Bottiglione, L. Afferrante, J. Monti, L. Pastewka, M. O. Robbins, J. A. Greenwood, Meeting the contact-mechanics challenge. *Tribol. Lett.* **65**, 118 (2017).
18. B. Weber, T. Suhina, T. Junge, L. Pastewka, A. M. Brouwer, D. Bonn, Molecular probes reveal deviations from Amontons' law in multi-asperity frictional contacts. *Nat. Commun.* **9**, 888 (2018).
19. A. Malekan, S. Rouhani, Model of contact friction based on extreme value statistics. arXiv:1709.01744 [cond-mat.stat-mech] (6 September 2017).
20. T. Baumberger, P. Berthoud, C. Caroli, Physical analysis of the state- and rate-dependent friction law. II. Dynamic friction. *Phys. Rev. B* **60**, 3928–3939 (1999).
21. L. Bureau, T. Baumberger, C. Caroli, Rheological aging and rejuvenation in solid friction contacts. *Eur. Phys. J. E* **8**, 331–337 (2002).
22. S. M. Rubinstein, G. Cohen, J. Fineberg, Contact area measurements reveal loading-history dependence of static friction. *Phys. Rev. Lett.* **96**, 256103 (2006).
23. O. Ben-David, S. M. Rubinstein, J. Fineberg, Slip-stick and the evolution of frictional strength. *Nature* **463**, 76–79 (2010).
24. V. Romero, E. Wandersman, G. Debrégeas, A. Prevost, Probing locally the onset of slippage at a model multicontact interface. *Phys. Rev. Lett.* **112**, 094301 (2014).
25. R. Sahli, G. Pallares, C. Ducottet, I. E. Ben Ali, S. Al Akhrass, M. Guibert, J. Scheibert, Evolution of real contact area under shear and the value of static friction of soft materials. *Proc. Natl. Acad. Sci. U.S.A.* **115**, 471–476 (2018).
26. T. Suhina, B. Weber, C. E. Carpentier, K. Lorincz, P. Schall, D. Bonn, A. M. Brouwer, Fluorescence microscopy visualization of contacts between objects. *Angew. Chem. Int. Ed.* **54**, 3688–3691 (2015).
27. T. Suhina, S. Amirjalayer, B. Mennucci, S. Woutersen, M. Hilbers, D. Bonn, A. M. Brouwer, Excited-state decay pathways of molecular rotors: Twisted intermediate or conical intersection? *J. Phys. Chem. Lett.* **7**, 4285–4290 (2016).
28. A. Gujrati, S. R. Khanal, L. Pastewka, T. D. B. Jacobs, Combining TEM, AFM, and profilometry for quantitative topography characterization across all scales. *ACS Appl. Mater. Interfaces* **10**, 29169–29178 (2018).
29. L. Bureau, T. Baumberger, C. Caroli, Non-amontons behavior of friction in single contacts. *Eur. Phys. J. E* **19**, 163–169 (2006).
30. L. Bureau, C. Caroli, T. Baumberger, Frictional dissipation and interfacial glass transition of polymeric solids. *Phys. Rev. Lett.* **97**, 225501 (2006).
31. J. F. Waters, P. R. Guduru, Mode-mixity-dependent adhesive contact of a sphere on a plane surface. *Proc. R. Soc. Lond. A Math. Phys. Sci.* **466**, 1303–1325 (2009).
32. S. M. Rubinstein, G. Cohen, J. Fineberg, Detachment fronts and the onset of dynamic friction. *Nature* **430**, 1005–1009 (2004).
33. J. K. Trømborg, H. A. Sveinsson, J. Scheibert, K. Thøgersen, D. S. Amundsen, A. Malthe-Sørenssen, Slow slip and the transition from fast to slow fronts in the rupture of frictional interfaces. *Proc. Natl. Acad. Sci. U.S.A.* **111**, 8764–8769 (2014).
34. K. Tian, D. L. Goldsby, R. W. Carpick, Rate and state friction relation for nanoscale contacts: Thermally activated Prandtl-Tomlinson model with chemical aging. *Phys. Rev. Lett.* **120**, 186101 (2018).
35. A. E. Filippov, J. Klafter, M. Urbakh, Friction through dynamical formation and rupture of molecular bonds. *Phys. Rev. Lett.* **92**, 135503 (2004).
36. P. Kokelaar, Friction melting, catastrophic dilation and breccia formation along caldera superfaults. *J. Geol. Soc. London* **164**, 751–754 (2007).
37. Y. Lavallée, T. Hirose, J. E. Kendrick, K.-U. Hess, D. B. Dingwell, Fault rheology beyond frictional melting. *Proc. Natl. Acad. Sci. U.S.A.* **112**, 9276–9280 (2015).
38. N. Otsu, A threshold selection method from gray-level histograms. *IEEE Trans. Syst. Man Cybern.* **9**, 62–66 (1979).

39. T. Förster, G. Hoffmann, Die Viskositatsabhängigkeit der Fluoreszenzquantenausbeuten einiger Farbstoffsysteme. *Z. Phys. Chem.* **75**, 63–76 (1971).

Acknowledgments: We thank C. Coulais and M. Bonn for helpful discussions. **Funding:** This work is part of the FOM–Programme Fundamental Aspects of Friction, financed by FOM/NWO. **Author contributions:** B.W. conducted the friction, visualization, and AFM experiments and the contact calculations. T.S. prepared the functionalized coverslips. B.W., T.S., A.M.B., and D.B. interpreted the data and wrote the manuscript. **Competing interests:** The authors declare that they have no competing interests. **Data and materials availability:** All data needed to evaluate the conclusions in the paper are present in the paper and/or the Supplementary Materials. Additional data related to this paper may be requested from the authors.

Submitted 17 October 2018
Accepted 11 February 2019
Published 5 April 2019
10.1126/sciadv.aav7603

Citation: B. Weber, T. Suhina, A. M. Brouwer, D. Bonn, Frictional weakening of slip interfaces. *Sci. Adv.* **5**, eaav7603 (2019).

Frictional weakening of slip interfaces

B. Weber, T. Suhina, A. M. Brouwer and D. Bonn

Sci Adv **5** (4), eaav7603.
DOI: 10.1126/sciadv.aav7603